Performance analysis of a horizontal axis wind turbine

Dalibor Rozehnal[1,*] and *Jakub* Hnidka[1]

[1]University of Defence in Brno, Kounicova 65, 612 00 Brno, Czech Republic

Abstract. This paper presents a performance analysis of a horizontal axis wind turbine with an atypical design. The performance analysis was performed by a measurement in a low-speed wind tunnel. The atypical design of the horizontal axis wind turbine mimics the design of a radial turbine. The wind turbine was, however, simplified by "removing" the conventional stationary parts of the radial turbine, such as portion of the case or guide vanes. The paper describes the measurement test bed and compares the performance of this atypical wind turbine with more conventional designs.

1 Introduction

The paper explores the performance of the atypical wind turbine (WT) design, which was derived from the design of a radial turbine. The paper presents results of the measurements in the wind tunnel, which were performed to verify the performance parameters of this atypical horizontal axis wind turbine (HAWT) and, ultimately, its suitability to harness the energy of wind and produce power. A growing effort can be observed in the industry to reduce its dependence on non-renewable energy sources [1-3]. This effort is coupled with accelerated advancements of renewable energy sources. Harvesting the power of the wind as a renewable power source is one of the most prominent methods in this field [3]. Effort to decrease of the dependency of the industry on non-renewable power sources is driven by an effort to reduce the emissions and the overall impact on the environment [4]. Increased amount of greenhouse gases in the atmosphere can have devastating impact on the sustainability of life on Earth [5]. The climate change can directly threaten the life in number of coastal states [6-8]. Energy harvested from wind is clean, sustainable and renewable. The design of machines capable of harvesting this energy and transforming it into other, more usable form of energy (typically, electricity) can vary significantly. Long-term research and practical experience revealed clear advantage of HAWT over other designs [9]. HAWT can range from simple to sophisticated solutions, with great reliability and, in the past decades, increasing power output [10, 11]. This in turn often renders other wind turbine design as obsolete.

Any design of the wind turbine can only harvest the energy of the wind passing through the disc of rotation of said wind turbine. From this standpoint, the most efficient HAWT

* Corresponding author: dalibor.rozehnal@unob.cz

design is a HAWT with three blades. The HAWT presented in this paper is a variation of the radial gas turbine, which was stripped from certain parts to simplify the design and improve both serviceability and economy of this WT. The measurements in the wind tunnel were performed to investigate the potential of this altered design.

2 Experimental Setup

The experimental equipment for the measurement of the WT aerodynamic characteristics is located in the circulation wind tunnel with the open testing area, see Fig. 1. The measuring stand is fully automated and enables us to measure the propeller aerodynamic characteristics, both static and dynamic.

WTs are tested by the standardized method. WT is fixed in the testing stand and is attached to the electric generator unit. The test bed is placed in the measurement section of the wind tunnel, see Fig. 1. At first required the velocity of the flow in the wind tunnel is set up, then the revolutions of wind turbine are continuously reduced until the min. RPM regime is reached, respectively when the wind turbine is stopped. Due to the very slow start up period (of about 120 s) and the short time of integration (0.1 s), during which the tested values are sampled, we can conclude that the testing is performed in quasi-static regime and very realistically corresponds to the real performance of the particular propeller. The time and energy savings represent the main advantage of this set-up.

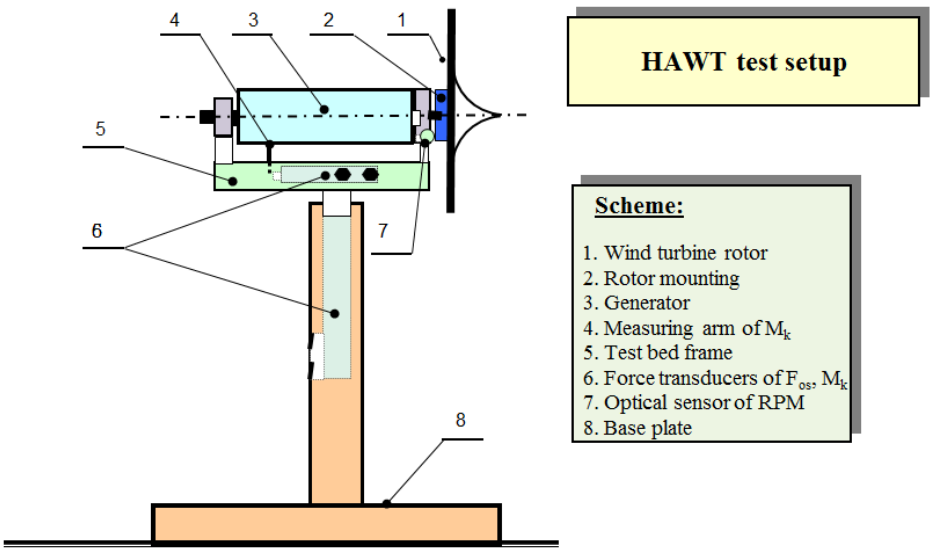

Fig. 1. Scheme of the HAWT test setup.

Table 1. Parameters of the wind tunnel.

Parameter	Notation	Value
Power output	P [kW]	18
Diameter of the measurement section	D [m]	0.6
Maximum velocity	v_{max} [m.s^{-1}]	42

Minimum velocity	v_{min} [m.s^{-1}]	2
Velocity deviation in measurement section	Δv [%]	<1.5

Parameters of the wind tunnel are listed in the Table 1. Parameters of the tested wind turbine along with the parameters of the power generator are listed in Table 2.

Table 2. Parameters of the test bed and of the tested wind turbine.

Parameter	Value
Output Power of continuously regulated el. generator	1.5 kW at 5,000 rpm
Stabilized DC power source	2.0 kW (30 V/60 A)
Electronic converter MGM of the brushless motor	45 V/80 A
Diameter of the tested rotor	21 in (0.53 m)
Range of rotor thrust measurement	<350 N
Range of rotor torque measurement	<16 N.m
Mass and dimensions of the test bed	75 kg (1100x600x1200 mm)

3 Theoretical analysis of the HAWT

HAWT harvests the kinetic energy of the wind passing through the plane of its rotation and converts it into the mechanical energy. The amount of the energy harvested and converted is directly proportional to the efficiency of the HAWT. In summary, the HAWT is machine generating mechanical energy on its output shaft – or it consumes negative amount of power. A propeller can be also operated in this so-called windmill regime.

In the design phase and for purposes of aerodynamic characteristics calculations of a HAWT, typically non-dimensional parameters are being used. These non-dimensional parameters can better capture the efficiency and quality of the proposed HAWT design and allow for comparison of different HAWT regimes of operation. The critical parameter, which ties the non-dimensional parameters and coefficients to the dimensional real aerodynamic forces is a velocity of the wind passing through the plane of rotation of HAWT.

4 Verification of parameters of proposed HAWT in wind tunnel

Forces acting on a measured object – HAWT, are transformed in transducers to electrical signal, which is then sampled in a 16-bit data acquisition card. The parameters measured were revolutions of the HAWT's rotor, axial force acting on the HAWT's rotor, its torque moment and the far wind velocity. The entire measurement chain is shown in Fig. 2. The measurement of all velocities was performed with a constant time-step of 10 kS/ch/s.

The data acquisition, with data processing, visualization and data logging was all programmed in LabVIEW. The system is introduced in [12]. The HAWT measured is shown in Fig. 2 and 5. HAWT's blades are bounded by two co-centric circles, which are connected from leading to trailing edge by two constant arcs with constant radius. The chord length of

each blade is 60 mm, the height is equal to 30 mm. The diameter of the rotor is 500 mm and it can be fitted with 20 blades in total. Additionally, the angle of attack of each blade can be adjusted in three settings (min, max, AVG) – see Fig. 6 and 7. To simplify the design and reduce the overall weight of the HAWT, the stator set up typically used in radial gas turbines was omitted.

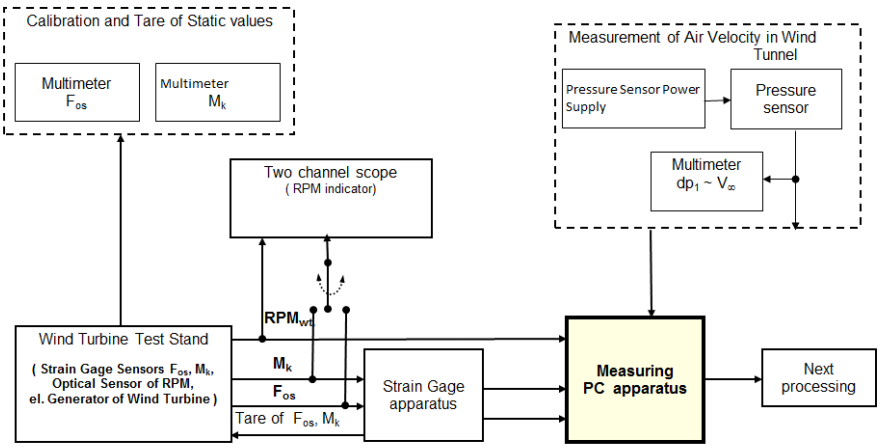

Fig. 2. Scheme of the measurement chain.

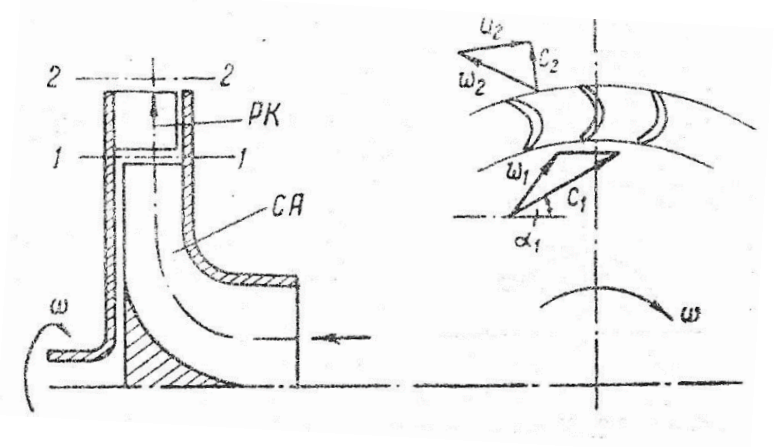

Fig. 3. Scheme of the radial centrifugal gas turbine. PK-radial impeller, CA-stator distribution channel.

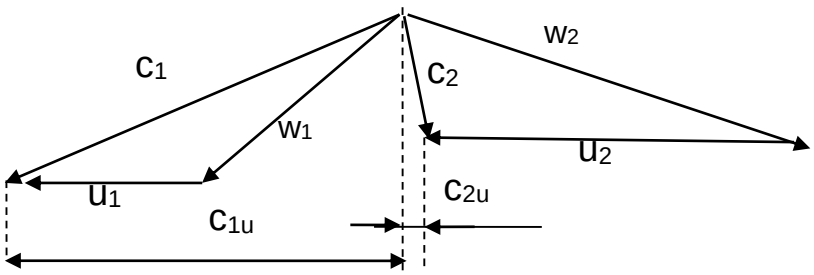

Fig. 4. Speed triangles on the wheel of the HAWT.

Basic computational formulas are as follows. The work of the air flowing through the HAWT ca be obtained as

$$W_{st} = c_{1u} \cdot u_1 + c_{2u} \cdot u_2 \tag{1}$$

The power of the air flowing through the HAWT

$$P_T = Q_m \, W_{stt} \tag{2}$$

The mass flow of the air is noted as Q_m, the density of the air as ρ, diameter of the HAWT's rotor is D, revolutions per second of the HAWT n, far flow velocity V_0, coefficient of axial force c_f, coefficient of power c_p and coefficient of torque moment c_m. Tip-speed ratio λ_0 can then be then expressed as

$$\lambda_o = \frac{\pi \cdot D \cdot n}{V_o} \tag{3}$$

The axial force (thrust) T, power produced by a HAWT N, its torque moment M and efficiency can then be calculated as following

$$T = \frac{1}{8} \cdot c_f \cdot \rho \cdot \pi \cdot D^2 \cdot V_o^2 \tag{4}$$

$$N = \frac{1}{8} \cdot c_p \cdot \rho \cdot \pi \cdot D^2 \cdot V_o^3 \tag{5}$$

$$M = \frac{1}{16} \cdot c_m \cdot \rho \cdot \pi \cdot D^3 \cdot V_o^2 \tag{6}$$

$$\eta_m = \frac{M \cdot \Omega}{T \cdot V_o} = \frac{c_m}{c_f} \cdot \lambda_o \tag{7}$$

The axial force coefficient c_f, power coefficient c_p and torque moment coeffcient c_m plotted against tip-speed ratio form the aerodynamic characteristics of HAWT. This characteristics then shows the aerodynamic quality of the proposed design and impact its range of application.

Fig. 5. Measurement setup during HAWT performance verification in the measurement section of the wind tunnel.

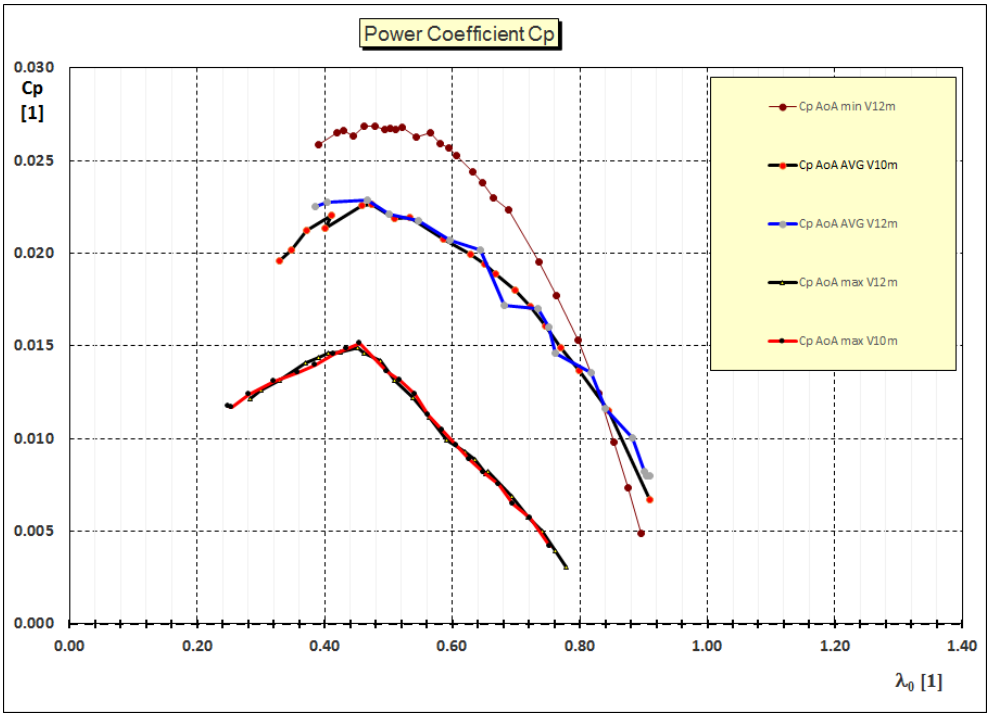

Fig. 6. Power coefficient dependency on tip-speed ratio λ_0 and impact of the change of the angle of attack on the results.

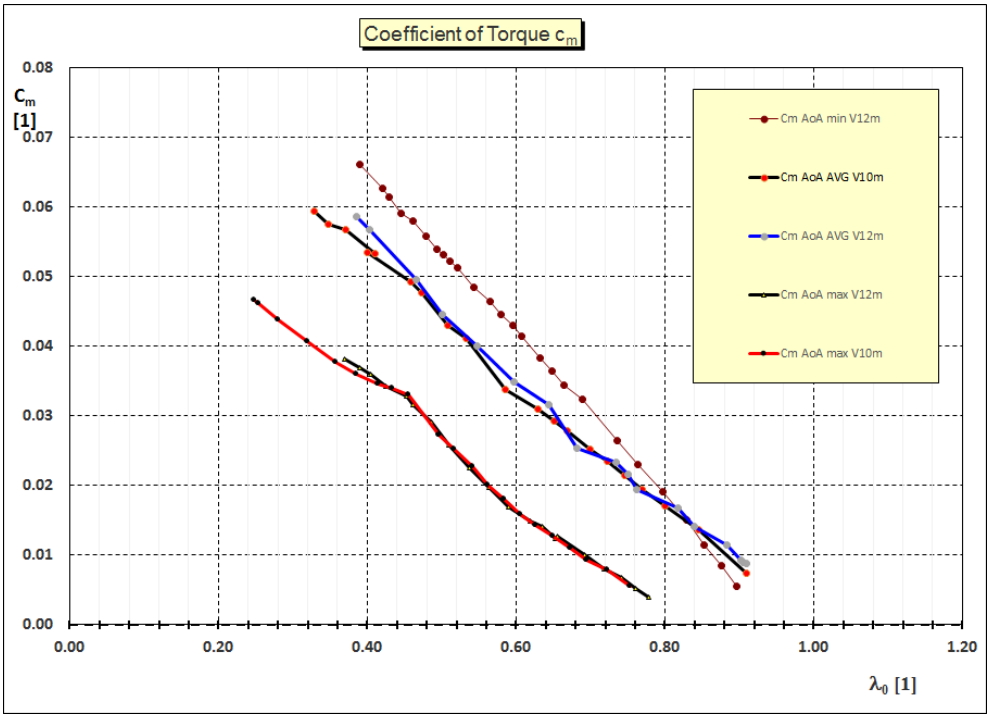

Fig. 7. Torque characteristics and impact of modifiable angle of attack of all blades.

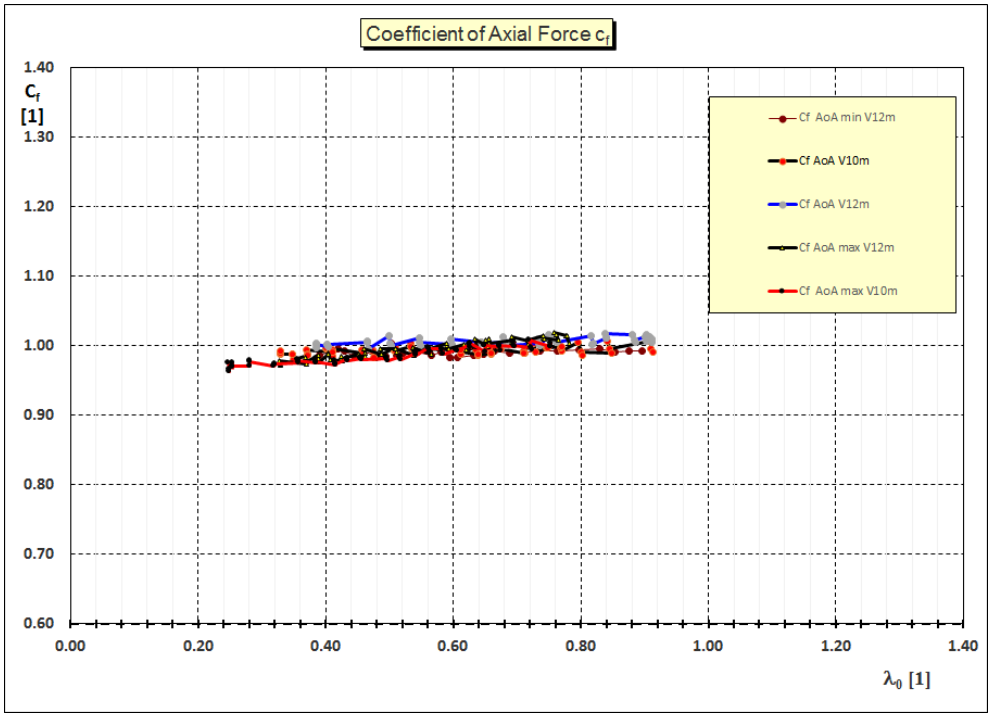

Fig. 8. Coefficient of axial force plotted against tip-speed ratio λ_0. The impact of variable angle of attack of all blades can be clearly seen from both graphs.

5 Conclusion

The results of the measurement of the HAWT in the wind tunnel were plotted against tip-speed ratio in a non-dimensional form. The resulting characteristics contain the power c_P, axial force c_F and torque moment c_M characteristics impacted by a different setting of angle of setting of HAWT blades. Fig. 6 and Fig. 7 both show clear dependency of a power and torque moment characteristics on both tip-speed ratio and angle of setting of HAWT blades. The axial force, as shown in Fig. 8 is independent on tip-speed ratio and angle of setting. The value of axial force coefficient was around 1.0 in the entire range of measurement. The value of axial force coefficient provides vital input into design phase of the HAWT, especially FEM analysis and strength to weight optimization. Power and moment coefficients provide necessary information about the power capabilities of the HAWT. A simplified rotor geometry proved to be less efficient than more conventional designs. However, the lowered efficiency was to be expected due a fairly simple initial design of the rotor blades. Improved and more complex geometry of the rotor blades will likely produce better results. The range of revolutions, in which the HAWT can operate, can be affected by the geometry of the rotor blades as well.

This research was performed with a support of TECHNOFIBER.

References

1. A. Q. Al-Shetwi, M. A. Hannan, K. P. Jern, M. Mansur, T.M.I. Mahila, Grid-connected renewable energy sources: Review of the recent integration requirements and control methods, Journal of Cleaner Production, **253**, 1-17 (2019)
2. F. Liu, S. Tait, A. Schellart, M. Mayfield, J. Boxall, Reducing carbon emissions by integrating urban water systems and renewable energy sources at a community scale, Renewable and Sustainable Energy Reviews, **123**, 1-14 (2020)
3. A Colmenar-Santos, A.-M. Munoz-Gomez, E. Rosales-Asensio, A. Lopez-Rey, Electric vehicle charging strategy to support renewable energy sources in Europe 2050 low-carbon scenario, Energy, **183**, 1-14 (2019)
4. H. Cai, S. Qu, M. Wang, Changes in China's carbon footprint and driving factors based on newly constructed time series input–output tables from 2009 to 2016, Science of The Total Environment, **711**, 1-13 (2020)
5. S. Chen, H. Long, B. Chen, K. Feng, K. Hubacek, Urban carbon footprints across scale: Important considerations for choosing system boundaries, Applied Energy, **259**, 1-12 (2020)
6. Y. Zhang, Y. Wang, Y. Chen, F. Liang, H. Liu, Assessment of future flash flood inundations in coastal regions under climate change scenarios—A case study of Hadahe River basin in northeastern China, Science of Total Environment, **693**, 1-11 (2019)
7. D. J. Lieske, T. Wade, L. A. Roness, Climate change awareness and strategies for communicating the risk of coastal flooding: A Canadian Maritime case example, Estuarine, Coastal and Shelf Science, **140**, 1-12 (2014)
8. R. J. Nicholls, Coastal flooding and wetland loss in the 21st century: changes under the SRES climate and socio-economic scenarios, Global Environmental Change, **14**, 69-86 (2004)
9. C.-J. Bai, W-Ch. Wang, Review of computational and experimental approaches to analysis of aerodynamic performance in horizontal-axis wind turbines (HAWTs), Renewable and Sustainable Energy Reviews, **63**, 506-519 (2016)
10. W. Tjiu, T. Marnoto, S. Mat, M. H. Ruslan, K. Sopian, Darrieus vertical axis wind turbine for power generation II: Challenges in HAWT and the opportunity of multi-megawatt Darrieus VAWT development, Renewable Energy, **75**, 560-571 (2015)
11. L. Zhiqiang, W. Yunke, H. Jie, Z Zhihong, Ch. Wenqi, The study on performance and aerodynamics of micro counter-rotating HAWT, Energy, **161**, 939-954 (2018)
12. J. Hnidka, D. Rozehnal, Pressure field in measurement section of wind tunnel, MATEC Web of Conferences, **107**, 1-10 (2017)